Radiation Oncology

RESEARCH

Open Access

Bone matching versus tumor matching in image-guided carbon ion radiotherapy for locally advanced non-small cell lung cancer

Jing Mi[1,2,3,4,5,6], Shubin Jia[1,2,3,4,5,6], Liyuan Chen[4,5,6], Yaqi Li[1,2,3,4,5,6], Jiayao Sun[2,3,7], Liwen Zhang[2,3,7], Jingfang Mao[1,2,3], Jian Chen[1,2,3], Ningyi Ma[1,2,3], Jingfang Zhao[2,3,7*] and Kailiang Wu[1,2,3,4,5,6*]

Abstract

Background and purpose This study evaluates the dosimetric impact of tumor matching (TM) and bone matching (BM) in carbon ion radiotherapy for locally advanced non-small cell lung cancer.

Materials and methods Forty patients diagnosed with locally advanced non-small cell lung cancer were included in this study. TM and BM techniques were employed for recalculation based on re-evaluation computed tomography (CT) images of the patients, resulting in the generation of dose distributions: Plan-T and Plan-B, respectively. These distributions were compared with the original dose distribution, Plan-O. The percentage of the internal gross tumor volume (iGTV) receiving a prescription dose greater than 95% (V95%) was evaluated using dose-volume parameters. Statistical analysis was performed using a paired signed-rank sum test. Additionally, the study investigated the influence of tumor displacement, volume changes, and rotational errors on target dose coverage.

Results The median iGTV V95% values for the Plan-O, Plan-T, and Plan-B groups were 100%, 99.93%, and 99.60%, respectively, with statistically significant differences observed. TM demonstrated improved target dose coverage compared to BM. Moreover, TM exhibited better target coverage in case of larger tumor displacement. TM's increased adjustability in rotation directions compared to BM significantly influenced dosimetric outcomes, rendering it more tolerant to variations in tumor morphology.

Conclusion TM exhibited superior target dose coverage compared to BM, particularly in cases of larger tumor displacement. TM also demonstrated better tolerance to variations in tumor morphology.

Keywords Carbon ion radiotherapy, Tumor matching, Bone matching, Lung cancer

*Correspondence:
Jingfang Zhao
jingfang.zhao@sphic.org.cn
Kailiang Wu
wukailiang@aliyun.com
[1]Department of Radiation Oncology, Shanghai Proton and Heavy Ion Center, Fudan University Cancer Hospital, NO. 4365 Kang Xin Road, Shanghai 201315, China
[2]Shanghai Key Laboratory of Radiation Oncology , Shanghai 201315, China
[3]Shanghai Engineering Research Center of Proton and Heavy Ion Radiation Therapy, Shanghai 201315, China
[4]Department of Radiation Oncology, Fudan University Shanghai Cancer Center, Shanghai 200032, China
[5]Department of Oncology, Shanghai Medical College, Fudan University, Shanghai 200032, China
[6]Shanghai Clinical Research Center for Radiation Oncology, Shanghai, China
[7]Department of Medical Physics, Shanghai Proton and Heavy Ion Center, Shanghai 201315, China

Introduction

Lung cancer stands as the leading cause of cancer-related mortality globally [1]. Among lung cancer cases, approximately 85% are attributed to non-small cell lung cancer (NSCLC) [2]. For patients with locally advanced NSCLC (LA-NSCLC), radiation therapy serves as a primary treatment modality [3]. In addition to conventional photon radiotherapy, particle radiotherapy has emerged as a promising approach, leveraging the unique characteristics of the "Bragg peak" phenomenon [4–6]. Carbon ion radiotherapy (CIRT) has gained recognition as a safe and efficacious treatment option for NSCLC, offering superior dose distribution compared to traditional photon radiotherapy [7–9]. However, particle radiotherapy, including CIRT, presents inherent challenges. Anatomical variations between treatment fractions can significantly influence the deposition profile of particle beams, particularly impacting the position of the Bragg peak. Such deviations may lead to substantial variations in the delivered doses to target tissues and organs at risk [10, 11]. The susceptibility of dose distribution to anatomical changes underscores the critical role of integrating image-guided radiotherapy (IGRT) into particle radiotherapy protocols. IGRT facilitates precise and adaptive treatment delivery, enabling clinicians to account for and mitigate the impact of anatomical variations during the course of treatment [12].

Medical imaging modalities, including two-dimensional (2D) planar imaging, CT, cone-beam CT (CBCT), magnetic resonance imaging (MRI), among others, play a pivotal role in IGRT for tumor localization [13]. These imaging techniques are utilized to compare current treatment conditions with those established during radiotherapy planning, facilitating necessary adjustments to guide subsequent fractions of radiotherapy. Image registration is essential in this process to determine interfractional positioning errors [14]. Bone matching is often preferred in IGRT because bony structures are less prone to deformation and provide higher contrast in imaging, allowing for more reliable and precise registration. Furthermore, it was believed that the misalignment of the bone would cause more range deviations than other soft tissues, as the bone was considered to have higher density. As previously noted, carbon ions demonstrate a distinct pattern of dose deposition defined by water equivalent path lengths (WEL). Given that WEL varies with material thickness and density, bone matching is frequently employed in CIRT [15–17]. However, different image registration methods may yield significant variations in position errors, registration times, and resulting dose distributions [18, 19]. TM has emerged as a promising alternative to BM, particularly in cases of early lung and pancreatic cancers undergoing passive scattering CIRT [15, 20]. Moreover, due to the interplay effect between anatomical changes and beam delivery, pencil beam scanning (PBS) techniques are more susceptible than passive scattering techniques to the influence of respiration-induced tumor motion [21].

To the best of our knowledge, there is a paucity of studies investigating the effect of different registration modalities on locally advanced non-small cell lung cancer (LA-NSCLC).

In this study, we aimed to address this gap by conducting an investigation into the impact of TM and BM on LA-NSCLC. Our study cohort comprised 40 patients diagnosed with LA-NSCLC who underwent PBS CIRT. For each patient, we conducted four-dimensional (4D) CT scans, with both the plan CT and re-evaluation CT reconstructed as average CTs. Subsequently, we aligned the acquired re-evaluation CT with the corresponding plan CT using both TM and BM techniques. Then, we recalculated the dose distributions in the treatment planning system to assess the dosimetric effects of TM and BM in the treatment of LA-NSCLC.

Materials and methods

Patient selection

Forty patients with LA-NSCLC were included in this study. These patients received PBS CIRT at Shanghai Proton and Heavy Ion Center from July 2016 to June 2020. Patients were 18 to 80 years old of any sex and had an ECOG 0–2 at the time of initial radiotherapy. Patients who underwent replan were excluded due to substantial anatomical changes, as neither registration method could meet the clinical treatment requirements.

Image acquisition

A vacuum bag, thermoplastic mask, or body shield was used to secure patients' positions. The supine or prone position was determined based on the target position of each patient. The plan CT and re-evaluation CT were acquired using two Siemens SOMATOM Definition AS scanners, and 4DCT were performed using the Anzai respiratory control system, with a scanning layer thickness of 3 millimeters. The scans encompassed the region from the mandible to the adrenal glands, covering the tumors, entire lungs, neck, and all other organs and tissues involved in the treatment field. In-room CT scans were conducted before the initial treatment and weekly throughout the treatment course, employing the same scanning conditions as the planning CT. The CT images from the final week of re-evaluation were chosen for analysis in this study.

Planning

The 4DCT were sorted into ten respiratory phases, representing a complete respiratory cycle. Before treatment planning, tumor movement was investigated in

ten phases of 4DCT. During treatment, patients undergo beam delivery within the respiratory-gated window spanning from expiration 20% (Ex20%) to inspiration 20% (In20%). Therefore, we calculated the average CTs of the three phases (Ex20%, 0%, and In20%) for planning. Internal gross tumor volume (iGTV) and the tumor size visible on CT, including the primary tumor in the lung, metastatic hilum, and mediastinal lymph nodes, were delineated by an experienced radiotherapy oncologist. Clinical tumor volume (CTV) was defined as the iGTV expanded by 0.6–0.8 cm. Planning tumor volume generally expands from CTV by 0.7–1.5 cm in the beam direction and 0.5–0.7 cm in other directions. Contrast-enhanced CT and positron emission tomography were used as a reference when delineating the region of interest on plan CT. The contours on the re-evaluation CT were transferred from the original CT using deformable registration in MIM software. These contours were then reviewed and adjusted by the doctor.

All CIRT plans were generated using a Syngo® treatment planning system (VB13, Siemens Health Solution, Erlangen, Germany). The median prescription dose was 79.2 (64–83.6) Gy (relative biological effectiveness, RBE), delivered in fractions of 3–4 Gy (RBE) over 16–22 sessions.

Treatment

All patients receive treatment once daily. Before each session, two orthogonal X-ray images are taken to verify and align the patient based on skeletal structures, with a positional accuracy requirement of less than 3 mm and a rotational tolerance of ±3°. The treatment couch can move within a range of ±20 cm in the X and Y directions, and from 0 to 30 cm in the Z direction. In terms of rotation, it can rotate ±15° in the roll direction and from 6.9° to -15° in the pitch direction. The table can also rotate from 270° to 170°/-10°. The beam angles in the treatment room are fixed at 45° and 90°, and the incident angle is adjusted by rotating the treatment couch.

Image registration methods

We used the Siemens Syngo® treatment planning system to implement automatic BM, and manually adjusted according to the position of the vertebrae, sternum, and ribs. TM was conducted using the MIM software. Initially, BM was automatically executed in the software, followed by contour-based alignment using the iGTV on the plan CT. These two steps were automatically completed by the software algorithm. Subsequently, the methods were assessed by a senior physicist and physician.

Data analysis

For each patient, three types of dose distributions were obtained:

a) Plan-O: The original plan calculated on the plan CT.
b) Plan-T: The original treatment plan recalculated on the re-evaluation CT using the TM method for registration.
c) Plan-B: The original treatment plan recalculated on the re-evaluation CT using the BM method for registration.

In this study, we used dosimetric parameters including V95% (the volume of the target area receiving more than 95% of the prescribed dose), D95 (the dose corresponding to 95% of the target volume), D99 (the dose corresponding to 99% of the target volume), median dose, and the homogeneity index (HI) to assess the dose coverage of the target area. Due to variations in the prescribed doses among the enrolled patients, we normalized the median dose, D95 and D99 by dividing them by their respective prescribed doses and expressed these doses as percentages of the corresponding prescription dose levels. Throughout the following text, we continue to refer to these as the relative median dose, relative D95 (D95%) and relative D99 (D99%). A V95% >95% was considered a clinically acceptable level.

The dose–volume histogram analysis of organs at risk (OARs) included the volume of normal lung irradiated with 5, 10, and 20 Gy (RBE) (V5, V10, V20), mean dose to the lung and heart, the maximum dose to the spinal cord, mean and maximum dose to the esophagus, and maximum dose to the main bronchial tree.

In addition to dosimetric parameters, we also collected clinical parameters such as fraction dose, initial iGTV volume, changes in iGTV, relative changes in iGTV, and rotational errors to explore their impact on dose distribution.

Tumor displacement was defined as the difference from the geometric center of the iGTV, which could be obtained from the MIM between re-evaluation CT and plan CT in three directions (X, right-left; Y, anterior-posterior; Z, superior-inferior):

$$\text{Tumor displacement} = \sqrt{(X_2\text{-}X_1)^2+(Y_2\text{-}Y_1)^2+(Z_2\text{-}Z_1)^2}$$

After the registration was completed, we recorded the setup errors of the two registration methods in six directions, including translation errors (X, Y, Z) and the rotation errors around the X-, Y-, and Z-axis, respectively (pitch, table, roll). $\triangle$Pitch, $\triangle$table, and $\triangle$roll were defined as the absolute values of the difference between the rotation error of TM and BM. All WELs were measured from the body surface to the isocenters of each beam's direction plane. Each case had two to three different beam directions. We calculated the square of the linear distance (SLD) between the tumor center (X, Y, Z) and the isocenter (x, y, z), reflecting the difference in

tumor localization between the recalculated and original plans:

$$\mathrm{SLD}=(\mathrm{x\text{-}X})^2+(\mathrm{y\text{-}Y})^2+(\mathrm{z\text{-}Z})^2$$

To investigate the factors that influence the different dosimetric outcomes, we defined two iGTV-related parameters:

$$\Delta\, V95\%_T \;=\; V95\%(Plan-T) \;-\; V95\%(Plan-O)$$

$$\Delta\, V95\%_B \;=\; V95\%(Plan-B) \;-\; V95\%(Plan-O)$$

The collected clinical parameters were then used to correlate with these two parameters.

Statistical methods

The statistical significance of dose differences between Plan-O, Plan-T, and Plan-B was compared using the paired signed-rank test. Differences in WEL, SLD, translation error, and rotation error were assessed using the paired signed-rank sum test. Rank correlation analysis was used to investigate the correlation between different physical parameters and V95%. A p-value < 0.05 was considered statistically significant.

Table 1 Patient characteristics ($n=40$)

Patient characteristics	Number or Value
Age	
Median	66
Range	46–80
Sex	
Male	31
Female	9
Smoke	
Yes	30
No	10
Tumor location	
LLL	5
LUL	11
RLL	4
RUL	16
RML	4
Prescription dose (Gy(RBE))	
Median	79.2
Range	64-83.6
Interval day	
Median	38.5
Range	26–76
Fraction dose (Gy(RBE))	
Median	3.75
Range	3.3-4
Changes of iGTV (cm^3)	
Median	0.545
Range	-9.83-73.54
Relative change in iGTV (%)	
Median	6.86
Range	0.28–22.03

RBE, relative biological effectiveness; iGTV, internal gross tumor volume. LLL, left lower lobe; LUL, left upper lobe; RLL, right lower lobe; RUL, right upper lobe; RML, right middle lobe

Results

The age, sex, tumor location, prescription dose, interval (time interval between plan and re-evaluation CT scans), and tumor changes in these patients are shown in Table 1.

The dosimetric parameters are presented in Table 2.

The dosimetric parameters of the target iGTV and CTV in the Plan-O, Plan-T, and Plan-B groups showed statistically significant differences, except for the relative median dose of CTV between Plan-O and Plan-T. Compared to Plan-O, both Plan-T and Plan-B exhibited inadequate target coverage, but Plan-T performed slightly better than Plan-B. Only one case for Plan-T, but four for Plan-B, did not reach acceptable levels. The variations among the three dose distributions are explicitly illustrated in Fig. 1.

A comparison of setup errors is presented in Table 3. Two registration methods had no significant difference in translation error but showed significant differences in the three rotation directions.

Our study findings indicate no differences in WEL between the two registration methods. However, there were differences in WEL observed between the re-evaluation CT and the original CT, regardless of the registration method used. The WEL measured using TM increased by an average of 0.28 mm compared to the original plan, while the WEL measured using BM increased by an average of 0.25 mm compared to the original plan (Plan-O vs. Plan-T, $P<0.001$; Plan-O vs. Plan-B, $P<0.001$; Plan-T vs. Plan-B, $P=0.4105$). However, from a statistical standpoint, only Plan-O and Plan-B showed a significant difference. For Plan-O, Plan-T, and Plan-B, the mean SLD is 0.321 cm^2, 0.560 cm^2, and 0.579 cm^2 (Plan-O vs. Plan-T, $P=0.6380$; Plan-O vs. Plan-B, $P=0.0026$; Plan-T vs. Plan-B, $P=0.0878$).

In Table 4, both the volume change of the tumor and the rotation error in the X and Y directions in the TM had a significant effect on the dosimetric results. However, for BM, the volume change of the tumor does not have a large effect on the dosimetric results. Similarly, only the rotation error around the Y-axis significantly affects $\triangle V95\%_B$.

Figure 2 shows the relationship between the iGTV V95% and tumor displacement. The iGTV V95% displayed a downward trend when tumor displacement increased in both TM and BM but more slowly in TM.

Table 2 Dose–volume parameters of planned and recalculated dose

ROI	Parameters	Dose distribution		
		Plan-O	Plan-T	Plan-B
iGTV	V95% (%)	100	99.93*, **	99.60*
		(99.39–100)	(88.88–100)	(82.088-100)
	D95%	1.016	0.999*, **	0.994*
		(0.960–1.082)	(0.926–1.057)	(0.915–1.054)
	D99%	1.008	0.978*, **	0.967*
		(0.953–1.073)	(0.769–1.031)	(0.790–1.024)
	Relative median dose	1.037	1.033**	1.032*
		(1.008–1.110)	(1.008–1.110)	(0.982–1.103)
	HI	1.037	1.076*, **	1.080*
		(1.020–1.129)	(1.032–1.185)	(1.032–1.208)
CTV	V95%	100	99.67*, **	99.20*
		(99.58–100)	(95.918-100)	(93.46–100)
	D95%	1.080	1.052*, **	1.030*
		(1.025–1.172)	(0.957–1.143)	(0.924–1.136)
	D99%	1.047	0.989*, **	0.966*
		(0.997–1.154)	(0.611–1.113)	(0.668–1.104)
	Relative median dose	1.139	1.140**	1.037
		(1.085–1.211)	(1.093–1.181)	(1.082–1.187)
Lungs	V5 (%)	24.89	24.48	24.03
		(11.54–48.05)	(11.44–47.40)	(10.74–47.69)
	V20 (%)	16.37	17.17*	16.70
		(6.04–30.99)	(7.29–32.04)	(7.70-32.55)
	Mean dose (Gy(RBE))	9.43	9.68	9.71
		(3.76–15.36)	(4.62–16.50)	(4.49–17.56)
Heart	V40 (%)	2.76	2.61**	2.56
		(0-11.31)	(0-12.38)	(0-13.48)
	Mean dose (Gy(RBE))	3.48	3.55**	2.95
		(0.07–12.85)	(0.04–15.31)	(0.03–15.09)
Spinal cord	Max dose (Gy(RBE))	26.44	24.55	27.74
		(4.01–56.89)	(3.27–50.49)	(3.65–52.46)
Esophagus	Max dose (Gy(RBE))	74.62	75.98	74.95*
		(4.05–86.02)	(3.67–87.80)	(3.82–87.65)
	Mean dose (Gy(RBE))	13.26	12.03**	11.95
		(0.18–40.05)	(0.14–42.94)	(0.20-42.98)
Bronchial tree	Max dose (Gy(RBE))	83.38	85.05*, **	86.12*
		(4.58–89.80)	(5.23–95.55)	(3.22–96.54)

Data are presented as median (range)

D95% (D99%), the dose covering 95% (99%) of the iGTV or CTV as a ratio of the prescribed dose; V95%, percentage of target volume that included 95% of the prescribed dose area; V5 and V20, percentage of the total lung volume receiving 20 Gy(RBE) and 5 Gy(RBE); V40, percentage of the heart receiving 40 Gy(RBE)

* Indicates significant difference compared with the Plan-O

** Indicates significant difference compared with the Plan-B

Discussion and conclusion

Our findings revealed significant statistical differences in dosimetric parameters of the targets, with Plan-T demonstrating superior performance over Plan-B. Patients stand to benefit from the TM method, as it offers improved target coverage without significant compromise to normal tissue in the context of three-dimensional (3D) image-guided CIRT. Discrepancies in dose coverage were more pronounced within the target area compared to OARs across the three groups. Variations in dose delivery to critical structures such as the heart, esophagus, and bronchial tree were observed with different registration methods. Notably, TM, in contrast to BM, may potentially lead to dose escalation to the heart and esophagus. This escalation could be attributed to the proximity of the esophagus to the vertebrae and the substantial rotational errors associated with TM. Furthermore, instances where the target region was adjacent to the esophagus or heart resulted in an increase in target dose corresponding to a rise in OAR doses.

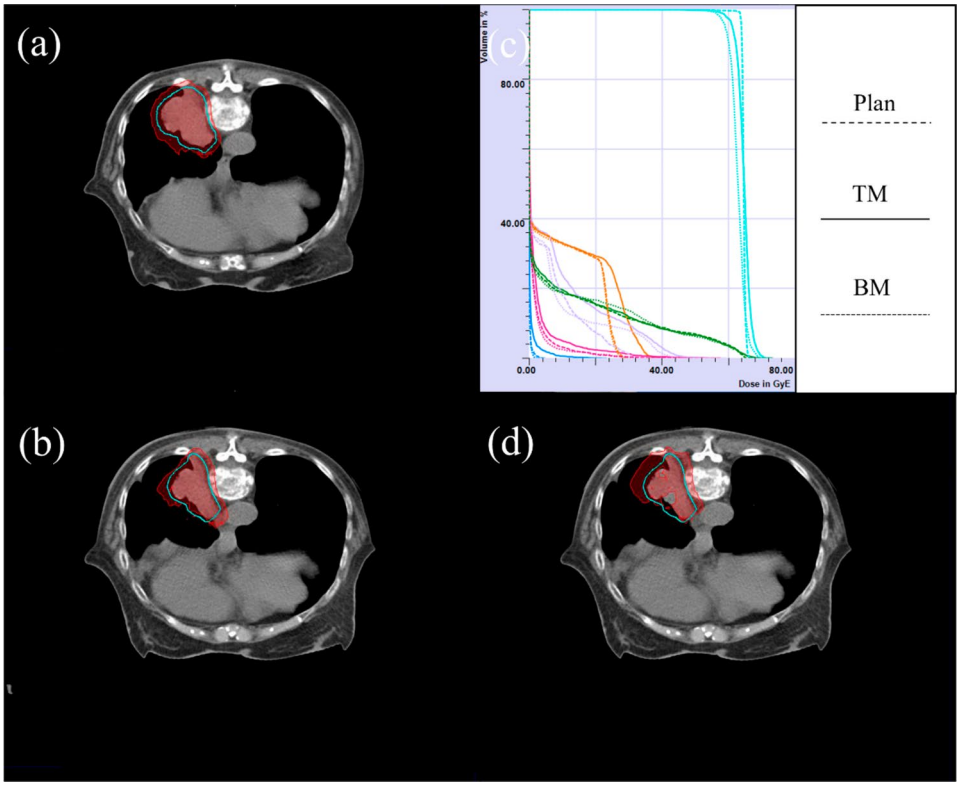

Fig. 1 Dose distributions of (**a**) Plan-O, (**b**) Plan-T, and (**d**) Plan-B. The blue contour represents the internal gross tumor volume, and the red shaded area represents the 95% prescribed dose coverage. (**c**), Dose-volume histogram

Table 3 Translation error and rotation error for TM and BM

Method	X (mm)	Y (mm)	Z (mm)	Pitch (°)	Table (°)	Roll (°)
TM	-0.27 ± 2.74	-0.33 ± 2.11	-0.89 ± 4.18	1.2 ± 1.0	1.1 ± 1.0	1.5 ± 1.2
BM	-0.55 ± 2.24	-0.07 ± 2.28	-0.91 ± 3.67	0.3 ± 0.9	0.5 ± 0.5	0.2 ± 0.5
P	0.4930	0.5678	0.8193	< 0.001	0.0034	< 0.001

Data are presented as mean ± Std

TM, tumor matching; BM, bone matching

X, Y, and Z represent the translation error in the left-right, anterior-posterior and superior-interior. Pitch, Table, and Roll represent the absolute values of rotation error around the X-, Y-, and Z- axis

Table 4 Correlation analysis of clinical parameters with iGTV V95%

Parameter	Spearman's *r*		*P*	
	$\triangle V95\%_T$	$\triangle V95\%_B$	$\triangle V95\%_T$	$\triangle V95\%_B$
Fraction dose Gy(RBE)	0.0717	-0.1175	0.6601	0.4701
Initial iGTV volume (cm^3)	0.2591	0.1401	0.1065	0.3885
Changes of iGTV (cm^3)	0.3254	0.2980	0.0405	0.0618
Relative changes of iGTV (%)	0.3316	0.2990	0.0366	0.0609
△pitch (°)	0.3481	0.2468	0.0277	0.1247
△table (°)	0.3850	0.4170	0.0142	0.0074
△roll (°)	0.1141	0.1313	0.4834	0.4194

$\triangle V95\%_T$, Differences of iGTV V95% between Plan-T and Plan-O; $\triangle V95\%_B$, Differences of iGTV V95% between Plan-B and Plan-O; △pitch, △table, and △roll, the difference between the rotation error around X-, Y-, and Z- axis of TM and BM

Previous studies have reported that TM may induce a larger change WEL compared to BM, leading to a dose shift [15]. However, our observations reveal that alterations in WEL within the same set of CT images remain largely consistent across different registration methods. In this study, WEL measured the calculated distance from the skin surface to the isocenter in each beam direction. Within this context, WEL measurements were limited

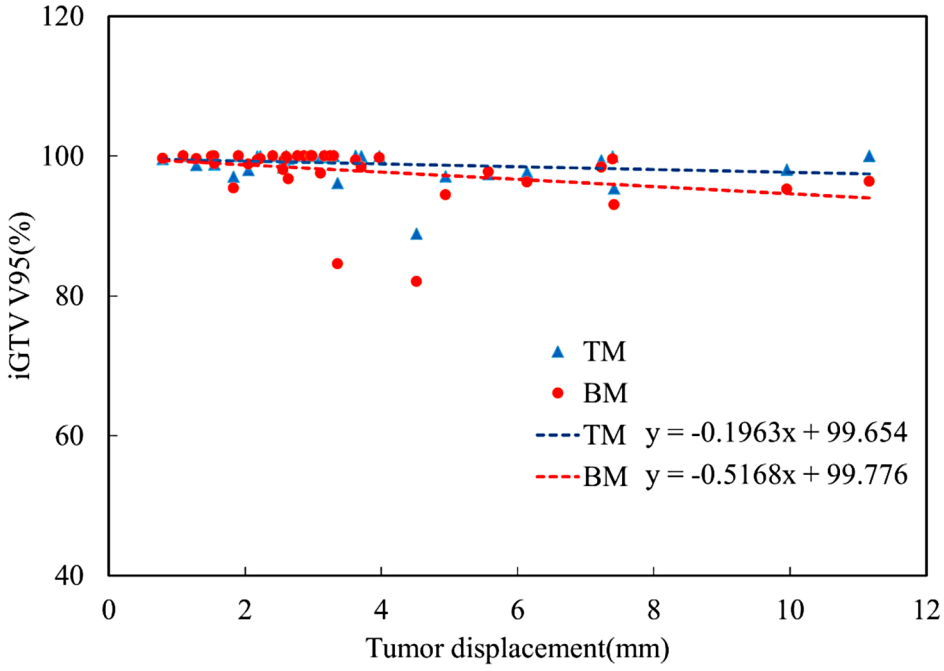

Fig. 2 The relationship between internal gross tumor volume V95% and tumor displacement

to only two to three specific directions. This restricted measurement range may result in the inability to observe changes in dose distribution in areas perpendicular to the beam direction. Furthermore, in cases involving multiple target areas, the isocenter of the beams was positioned between two or more tumors rather than within a single tumor. As a result, at certain beam angles, the measured WEL might not pass through the tumor region, potentially failing to accurately reflect changes in WEL between the tumor and the skin. Irrespective of whether TM or BM is employed, differences in the measured WELs compared to those in the original plan persist. Although the plan CT utilizes planning CT scanner and the re-evaluation CT utilizes in-room CT scanner, both devices have been commissioned to yield equivalent water depths under identical conditions. Hence, we infer that the noted variances could be ascribed to changes in patient anatomy.

We conducted separate evaluations to assess the impact of various physical parameters on the reduction of dose coverage in the target when utilizing different registration methods, including tumor volume change, fraction dose, and rotation error. Our data analysis revealed that the target dose was more sensitive to changes in tumor volume when employing TM compared to BM. Furthermore, rotation errors in the Y-direction significantly affected both TM and BM. Given that TM is based on BM, we posit that morphological changes in the tumor may contribute to differences in rotation between the two methods. These changes can alter the location of the tumor center, for which we further analyzed the SLD. Our findings indicate that the change in tumor position relative to the isocenter was more substantial in BM than in TM, resulting in inferior target dose distribution compared to TM. Although the TM was more sensitive to tumor changes, the TM was able to bring the dosimetric outcomes closer to the original plan by adjusting the rotation direction.

Scatter plots depicting the relationship between iGTV V95% and tumor displacement reaffirm the superiority of TM over BM, particularly in cases of larger tumor displacements. These findings align with previous research for early stage lung cancer [22].

Currently, our daily image-guided method employs 2D techniques. Prior to each treatment session, patients undergo orthogonal X-ray imaging in the treatment room to verify their positioning based on bony anatomy. X-rays typically exhibit lower resolution and contrast levels in comparison to CT scans, which may result in information loss and inaccuracies during registration. Primarily portraying skeletal structures, X-rays possess limited capacity to visualize soft tissues. Hence, BM is generally favored when aligning X-rays with CT scans. The transition to 3D image-guided CIRT offers significant advancements by providing detailed patient anatomical information, including tumor position, size, and morphology. This enhanced imaging capability facilitates recalculations of dose distributions and expands the available registration options to include both TM and bone matching BM, whereas previously, patients

were limited to BM in the context of 2D image-guided techniques.

In clinical practice, the incorporation of 3D image-guided CIRT allows us to select a more appropriate registration method combined with a six-degree-of-freedom couch for precise patient positioning, thereby optimizing treatment outcomes. Particularly for patients whose target dose coverage falls below clinical standards, adopting an alternative registration method that improves dose coverage can substantially reduce the need for clinical replanning and alleviate associated pressure.

However, it is important to acknowledge that while CT scans involve low-dose radiation, further validation is required to assess whether conducting an evaluation CT scan prior to each radiation treatment session impacts therapeutic efficacy for patients.

Closing of our discussion, we draw attention to the limitations of our study, such as the fact that inter-fractional changes were not considered. Previous studies have demonstrated the potential of accumulating dose distributions from re-evaluation CT acquired on different dates using deformable image registration (DIR) techniques [20, 22]. While dose accumulation allows for a more comprehensive recording of patients' daily anatomical variations, it is important to note that different DIR algorithms may yield varying cumulative doses, introducing additional uncertainty into the dose calculation process [23]. Despite the potential benefits of dose accumulation, our study did not employ this approach as our primary focus was to compare the performance of two registration methods rather than analyze patients' daily dose variations. Additionally, we did not evaluate free-breathing CT for comparison. While not accounting for tumor motion, they offer advantages in reducing time consumption and radiation dose exposure. Whether 4DCT or free-breathing CT should be selected remains to be studied and evaluated.

In conclusion, our study evaluated the dose distributions of the original plan, TM, and BM in CIRT for LA-NSCLC. Our findings indicate that regardless of the registration method employed, the recalculated dose distribution deviates from the original dose distribution. However, the utilization of TM effectively reduced variations in tumor location relative to the isocenter and demonstrated the potential to bring the dose distribution closer to the original plan. Furthermore, our analysis of dosimetric parameters for the targets revealed that TM achieved higher target dose coverage compared to BM, with this difference being more pronounced in cases of larger tumor displacement. These findings underscore the efficacy of TM in optimizing target dose coverage and maintaining treatment fidelity in the context of CIRT for LA-NSCLC.

Abbreviations

3D	three-dimensional
4DCT	four-dimensional computed tomography
BM	bone matching
CIRT	carbon ion radiotherapy
CT	computed tomography
CTV	clinical tumor volume
DIR	deformable image registration
IGRT	image-guided radiotherapy
iGTV	internal gross tumor volume
LA-NSCLC	locally advanced non-small cell lung cancer
NSCLC	non-small cell lung cancer
OARs	organs at risk
PBS	pencil beam scanning
RBE	relative biological effectiveness
SLD	square of the linear distance
TM	tumor matching
WEL	water equivalent path length

Acknowledgements
The authors thank the physicians and physicists at Shanghai Proton and Heavy Ion Center and Fudan University Shanghai Cancer Center during the data analysis.

Author contributions
WKL, ZJF, MJ have made substantial contributions to the proposal and design of the experiment. WKL, ZJF, MJF, CJ, MNY, MJ have provided important advice on the selection of the patients. MJ, JSB, CLY, ZLW, SJY have made substantial contributions to the acquisition. WKL ZJF, MJ contributed significantly to the interpretation. WKL, ZJF, MJ, LYQ have drafted the work or substantially revised it. All authors read and approved the final manuscript.

Funding
Project supported by the Shanghai Committee of Science and Technology, China (Grant No.23ZR1460200).

Data availability
Research data are available on request to the corresponding authors.

Declarations

Ethics approval and consent to participate
All institutional guidelines were followed. The study was approved by the Medical Ethics Committee of the Shanghai Proton Heavy Ion Hospital (SPHIC-THLC-2023-01(RS)).

Consent for publication
Not applicable.

Competing interests
The authors declare no competing interests.

Received: 17 May 2023 / Accepted: 20 November 2024
Published online: 18 December 2024

References

1. Sung H, Ferlay J, Siegel RL, et al. Global Cancer statistics 2020: GLOBOCAN estimates of incidence and Mortality Worldwide for 36 cancers in 185 Countries[J]. CA Cancer J Clin. 2021;71(3):209–49.
2. Goldstraw P, Ball D, Jett JR, et al. Non-small-cell lung cancer[J]. Lancet. 2011;378(9804):1727–40.
3. Turrisi AT 3rd, Bogart J, Sherman C, et al. The role of radiotherapy and chemotherapy for curative management of medically inoperable and stage III nonsmall cell lung cancer, and radiotherapy for palliation of symptomatic disease[J]. Respir Care Clin N Am. 2003;9(2):163–90.
4. Brown A, Suit H. The centenary of the discovery of the Bragg peak[J]. Radiother Oncol. 2004;73(3):265–8.
5. Klein C, Dokic I, Mairani A, et al. Overcoming hypoxia-induced tumor radioresistance in non-small cell lung cancer by targeting DNA-dependent

protein kinase in combination with carbon ion irradiation[J]. Radiat Oncol. 2017;12(1):208.
6. Grutters JP, Kessels AG, Pijls-Johannesma M, et al. Comparison of the effectiveness of radiotherapy with photons, protons and carbon-ions for non-small cell lung cancer: a meta-analysis[J]. Radiother Oncol. 2010;95(1):32–40.
7. Shirai K, Kawashima M, Saitoh JI, et al. Clinical outcomes using carbon-ion radiotherapy and dose-volume histogram comparison between carbon-ion radiotherapy and photon therapy for T2b-4N0M0 non-small cell lung cancer-A pilot study[J]. PLoS ONE. 2017;12(4):e0175589.
8. Kubo N, Saitoh JI, Shimada H, et al. Dosimetric comparison of carbon ion and X-ray radiotherapy for Stage IIIA non-small cell lung cancer[J]. J Radiat Res. 2016;57(5):548–54.
9. Hayashi K, Yamamoto N, Nakajima M, et al. Clinical outcomes of carbon-ion radiotherapy for locally advanced non-small-cell lung cancer[J]. Cancer Sci. 2019;110(2):734–41.
10. Houweling AC, Crama K, Visser J, et al. Comparing the dosimetric impact of interfractional anatomical changes in photon, proton and carbon ion radiotherapy for pancreatic cancer patients[J]. Phys Med Biol. 2017;62(8):3051–64.
11. Szeto YZ, Witte MG, Van Kranen SR, et al. Effects of anatomical changes on pencil beam scanning Proton plans in locally advanced NSCLC patients[J]. Radiother Oncol. 2016;120(2):286–92.
12. Li Y, Kubota Y, Tashiro M et al. Value of three-dimensional Imaging systems for image-guided Carbon Ion Radiotherapy[J]. Cancers (Basel) 2019;11(3).
13. Gupta T, Narayan CA. Image-guided radiation therapy: Physician's perspectives[J]. J Med Phys. 2012;37(4):174–82.
14. Moriya S, Tachibana H, Hotta K, et al. Feasibility of dynamic adaptive passive scattering proton therapy with computed tomography image guidance in the lung[J]. Med Phys. 2017;44(9):4474–81.
15. Sakai M, Kubota Y, Saitoh JI, et al. Robustness of patient positioning for interfractional error in carbon ion radiotherapy for stage I lung cancer: bone matching versus tumor matching[J]. Radiother Oncol. 2018;129(1):95–100.
16. Irie D, Saitoh JI, Shirai K, et al. Verification of Dose distribution in Carbon Ion Radiation Therapy for Stage I Lung Cancer[J]. Int J Radiat Oncol Biol Phys. 2016;96(5):1117–23.
17. Soukup M, Söhn M, Yan D, et al. Study of robustness of IMPT and IMRT for prostate cancer against organ movement[J]. Int J Radiat Oncol Biol Phys. 2009;75(3):941–9.
18. Cao X, Liu M, Zhai F, et al. Comparative evaluation of image registration methods with different interest regions in lung cancer radiotherapy[J]. BMC Med Imaging. 2019;19(1):100.
19. Liang X, Mailhot Vega RB, Li Z, et al. Dosimetric consequences of image guidance techniques on robust optimized intensity-modulated proton therapy for treatment of breast Cancer[J]. Radiat Oncol. 2020;15(1):47.
20. Kubota Y, Okamoto M, Shiba S, et al. Robustness of daily dose for each beam angle and accumulated dose for inter-fractional anatomical changes in passive carbon-ion radiotherapy for pancreatic cancer: bone matching versus tumor matching[J]. Radiother Oncol. 2021;157:85–92.
21. Boria AJ, Uh J, Pirlepesov F, et al. Interplay effect of Target Motion and Pencil-Beam scanning in Proton Therapy for Pediatric Patients[J]. Int J Part Ther. 2018;5(2):1–10.
22. Li Y, Kubota Y, Kubo N, et al. Dose assessment for patients with stage I non-small cell lung cancer receiving passive scattering carbon-ion radiotherapy using daily computed tomographic images: a prospective study[J]. Radiother Oncol. 2020;144:224–30.
23. Nenoff L, Ribeiro CO, Matter M, et al. Deformable image registration uncertainty for inter-fractional dose accumulation of lung cancer proton therapy[J]. Radiother Oncol. 2020;147:178–85.

Publisher's note